

Existence of steady gap solutions in rotating black hole magnetospheres

Amir Levinson & Noam Segev

Raymond and Beverly Sackler School of Physics & Astronomy, Tel Aviv University, Tel Aviv 69978, Israel

Under conditions prevailing in certain classes of compact astrophysical systems, the active magnetosphere of a rotating black hole becomes charge-starved, giving rise to formation of a spark gap in which plasma is continuously produced. The plasma production process is accompanied by curvature and inverse Compton emission of gamma rays in the GeV-TeV band, that may be detectable by current and future experiments. The properties of the gap emission have been studied recently using a fully general relativistic model of a local steady gap. However, this model requires artificial adjustment of the electric current which is determined, in reality, by the global properties of the magnetosphere. In this paper we map the parameter regime in which steady gap solutions exist, using a steady-state gap model in Kerr geometry, and show that such solutions are allowed only under restrictive conditions that may not apply to most astrophysical systems. We further argue that even the allowed solutions are inconsistent with the global magnetospheric structure. We conclude that magnetospheric gaps are inherently intermittent, and point out that this may drastically change their emission properties.

I. INTRODUCTION

A question of considerable interest in the theory of Poynting-flux outflows from black holes (BHs) [1, 2] is the nature of the plasma source in the magnetosphere. In difference from pulsars, in which free charges can be supplied to the magnetosphere by the rigid star along magnetic field lines that are anchored to its surface, in Kerr BHs there is no such an inherent plasma source. As discussed in some greater detail in the next section, plasma in the region enclosed between the inner and outer Alfvén surfaces must be continuously replenished by either some external agent or via pair cascades in a spark gap.

It has been argued that under conditions likely to prevail in many BH systems, both supermassive and stellar, formation of a spark gap is inevitable [3–6]. It has been further pointed out that the gap activity may be imprinted in the high-energy emission observed in these sources [3, 5–11]. The variable TeV emission detected in M87 [12, 13], a galaxy that harbours one of largest BHs in the universe, as well as in the radio galaxy IC 310 [14], has been regarded as being a plausible example of the signature of magnetospheric plasma production on horizon scales [3, 5, 9].

In essence, the gap is an inherent part of the global magnetospheric structure. Hence, a self-consistent analysis of magnetic outflows requires a proper account of the coupling between the gap and the force-free regions of the outflow. This can only be achieved, at least in principle, using global plasma simulations. While global PIC simulations have been performed recently for pulsars [15–17], they are expected to be far more involved in the case of black holes, since (i) a fully general relativistic scheme must be implemented, and (ii) unlike in pulsars, the origin of the magnetic field threading the BH is poorly understood, which reflects on the choice of boundary conditions. To avoid such complications, and still get some insight into the physics underlying plasma production in the gap, local gap solutions can be sought, in which the global magnetospheric structure is assumed

to be unaffected by the gap activity, while the magnetospheric current is treated as a free input parameter of the gap model.

In a recent series of papers [5–7], a fully general relativistic model of a steady gap has been developed and exploited to study the properties of magnetospheric emission. In this model the magnetospheric current was not treated as a free parameter, but rather adjusted, for any given choice of the remaining parameters, to keep the multiplicity at the value required by the closure condition (c.f., Eq. (26) in Ref [6]). The question then arises as to how restrictive are the conditions under which steady state solutions exist. This issue is of importance, as it might have drastic implications for the gap emission. The point is that in steady gaps that encompass the null surface the maximum power that can be released scales as h^4 with the gap width h [5]. Since the pair multiplicity in a steady gap cannot exceed unity, this implies that the gamma-ray luminosity emitted from a steady gap decreases rapidly as the intensity of the external radiation source, that provides the pair production opacity, increases. Such restrictions do not apply to intermittent gaps that can support a large magnetospheric current even when exposed to an intense radiation field. What are the limits on the output power of intermittent gaps is unclear at present. Future plasma simulations might be able to resolve this question.

In this paper we map the parameter regime in which local steady gap solutions exist, using a 1D model of a local magnetospheric gap in Kerr geometry. We find that such solutions require highly restrictive conditions, that may not apply to most astrophysical systems. Moreover, we argue that even the local steady solutions that are allowed in this model are inconsistent with the global magnetospheric structure. This implies that the plasma production region is dynamic, which may have far reaching consequences for the gap emission. In Sec. II we review the conditions under which gap formation is expected. In Sec. III we present the model, and in Sec. IV discuss the results. In sec. V we briefly remark on

the connection between the local model and the global structure. We conclude in Sec. VI.

II. CONDITIONS FOR VACUUM BREAKDOWN

An inherent feature of MHD outflows driven by a Kerr BH is the presence of a stagnation surface located between the inner and outer light cylinders (e.g., Refs [5, 11, 18, 19]). The reason is that the strong gravitational field of the black hole imposes an inward motion of plasma very near the horizon, regardless of the direction of the energy flux, whereas the plasma above the outer light cylinder must be flowing outwards. Consequently, the plasma in the causal magnetospheric region must be continuously replenished.

The injection of charges into the magnetosphere may be associated with the accretion process. Direct feeding seems unlikely, as charged particles would have to cross magnetic field lines on a timescale shorter than the accretion time in order to reach the polar outflow. Magnetic field irregularities, either inherent or forming by some macroscopic instabilities, can give rise to occasional loading of the magnetosphere. However, the timescale of such episodes may be considerably longer than the escape time of plasma in the inner magnetosphere (around the stagnation surface), so that some additional injection process may be required to maintain the local charge density above the Goldreich-Julian (GJ) value everywhere in the magnetosphere. In AGNs and microquasars this may be accomplished through annihilation of MeV photons emanating from the hot gas accreted into the black hole. We denote the luminosity of this radiation source, henceforth measured in Eddington units, by $l_\gamma = L_\gamma/L_{Edd}$, and its size, given in units of r_g , by $\tilde{R}_\gamma = R_\gamma/r_g$. For sufficiently high annihilation rate the resultant charge density can exceed the GJ value, keeping the magnetosphere force-free. At lower annihilation rates the magnetosphere will be starved and a gap should form.

The density of injected pairs can be estimated by equating the pair production rate with the escape rate. It is given roughly by $n_\pm \simeq \sigma_{\gamma\gamma} n_\gamma^2 r_g/3$ [3], where $n_\gamma \simeq 10^{22} m^{-1} \tilde{R}_\gamma^{-2} l_\gamma \text{ cm}^{-3}$ is the density of MeV photons, and $m = M_{BH}/M_\odot$ is the black hole mass in solar mass units. Complete screening requires $n_\pm > n_{GJ}$, here $n_{GJ} = \Omega B/(2\pi ec) = 2 \times 10^{11} B_8 (\Omega/\omega_H) m^{-1} \text{ cm}^{-3}$ denotes the GJ density, Ω is the angular velocity of magnetic surfaces, $\omega_H \simeq c/2r_g$ is the angular velocity of the black hole, $B = 10^8 B_8$ Gauss is the strength of the magnetic field near the horizon, and $e > 0$ is the magnitude of the electron charge. The later condition can be expressed as:

$$l_\gamma > 10^{-3} B_8^{1/2} (\Omega/\omega_H)^{1/2} (\tilde{R}_\gamma/30)^2. \quad (1)$$

For smaller values of l_γ the magnetosphere becomes charge starved and a gap forms.

The strength of the magnetic field near horizon can be estimated by assuming that it is in rough equipartition with the ram pressure in the disk. This yields

$$B \simeq 10^9 \dot{m}^{1/2} m^{-1/2} \text{ G}, \quad (2)$$

where $\dot{m} = \eta \dot{M} c^2 / \dot{L}_{Edd}$, with $\eta \simeq 0.1$ being the radiative efficiency, is the accretion rate in Eddington units.

In the RIAF regime the accretion flow is hot and the gamma ray luminosity can be estimated from an ADAF model, e.g., Ref [20], up to some uncertainty in the electron temperature. Adopting such a model yields a condition for the appearance of a gap: $\dot{m} < 4 \times 10^{-3} m^{-1/7}$ [3, 6]. At higher accretion rates the accretion disk spectrum cannot extend to high energies, as it is too cold. However, gamma-rays may originate from a tenuous corona, if present as widely believed, although no reliable constraints on the spectrum and luminosity of this coronal component have been imposed thus far. In principle, it could be that in sources that accrete at relatively high rates the magnetic field is much higher than in RIAF sources, while the gamma ray luminosity is suppressed. If indeed true it could mean that gap emission in such objects may be more intense than in RIAF sources.

III. A STATIONARY GAP MODEL

We construct a model describing a 1D, general relativistic stationary gap, that treats the electron-positron plasma as a two-beam fluid. The global magnetic field geometry adopted below is a split monopole geometry. The gap extends along a poloidal magnetic surface, characterized by an inclination angle θ . Gamma rays are produced by accelerating pairs via curvature emission and inverse Compton (IC) scattering, and in turn generate fresh pairs through their interaction with an ambient radiation field, given as input. It should be emphasized that these local steady gap solutions are applicable only in the region where ideal MDH breaks down. In the global picture additional forces are acting on the particles that are ignored here, which will determine the conditions outside the gap. The details are outlined in the following:

A. Background geometry

The background spacetime is described by the Kerr metric, here given in Boyer-Lindquist coordinates with the following notation:

$$ds^2 = -\alpha^2 dt^2 + g_{\varphi\varphi} (d\varphi - \omega dt)^2 + g_{rr} dr^2 + g_{\theta\theta} d\theta^2, \quad (3)$$

where

$$\begin{aligned} \alpha^2 &= \frac{\Sigma \Delta}{A}; & \omega &= \frac{2ar_g r}{A}; & g_{rr} &= \frac{\Sigma}{\Delta}; \\ g_{\theta\theta} &= \Sigma; & g_{\varphi\varphi} &= \frac{A}{\Sigma} \sin^2 \theta, \end{aligned} \quad (4)$$

with $\Delta = r^2 + a^2 - 2r_g r$, $\Sigma = r^2 + a^2 \cos^2 \theta$, $A = (r^2 + a^2)^2 - a^2 \Delta \sin^2 \theta$, and $r_g = GM/c^2$ denotes the gravitational radius. The parameter $a = J/M$ represents the specific angular momentum. The determinant of the matrix $g_{\mu\nu}$ is given by $\sqrt{-g} = \Sigma \sin \theta$. The angular velocity of the black hole is defined as $\omega_H = \omega(r = r_H) = \tilde{a}/2r_H$, where $\tilde{a} = a/r_g$ denotes the dimensionless spin parameter, and $r_H = r_g + \sqrt{r_g^2 - a^2}$ is the radius of the horizon. Henceforth, all lengths are measured in units of r_g and time in units of r_g/c , so we set $c = r_g = 1$ unless explicitly stated otherwise.

To avoid the singularity on the horizon, we find it convenient to transform to the tortoise coordinate ξ , defined by $d\xi = (r^2 + a^2)dr/\Delta$. It is related to r through:

$$\xi(r) = r + \frac{1}{\sqrt{1 - \tilde{a}^2}} \left[r_+ \ln \left(\frac{r}{r_+} - 1 \right) - r_- \ln \left(\frac{r}{r_-} - 1 \right) \right], \quad (5)$$

with $r_{\pm} = 1 \pm \sqrt{1 - \tilde{a}^2}$. Note that $\xi \rightarrow -\infty$ as $r \rightarrow r_H = r_+$.

B. Gap electric field

We implicitly assume that the gap forms a small perturbation in the force-free magnetosphere, in the sense that the potential drop across the gap is much smaller than the full vacuum potential. We can then ignore the variation in Ω in the gap and, for every magnetic flux surface, define the electric field in the corotating frame as $F'_{\mu t} = F_{\mu t} + \Omega F_{\mu\varphi}$. In general it satisfies Equation A5, with the GJ density defined explicitly in Equation A6. In order to compute the gap structure in our formalism, the magnetic field geometry needs to be specified. In what follows we adopt a split monopole geometry, defined by $A_\varphi = B_H \sqrt{A_H} (1 - \cos \theta)$, where $B_H = 10^8 B_8$ G denotes the strength of the magnetic field on the horizon, and $A_H \equiv A(r = r_H) = (r_H^2 + a^2)^2 = 4(1 + \sqrt{1 - \tilde{a}^2})^2$ in our units ($4r_g^2 r_H^2$ in full units). With this choice $F_{r\varphi} = 0$ and $F_{\theta\varphi} = B_H \sqrt{A_H} \sin \theta$. Note that in the ZAMO frame the radial magnetic field is given by $B_r = F_{\theta\varphi}/\sqrt{A} \sin \theta = B_H \sqrt{A_H}/A$, and the non-corotating electric field by $E'_r = \sqrt{A} F'_{rt}/\Sigma$. We find it convenient to use the electric flux function $\Phi_E = \sqrt{A} E'_r$ (which is essentially the electric flux per solid angle, as measured in the ZAMO frame). Then, Gauss' law, Eq. (A5), reduces to (see Eq. (A7))

$$\partial_\xi \Phi_E = \frac{4\pi \Sigma \Delta}{r^2 + \tilde{a}^2} (\rho_e - \rho_{GJ}), \quad (6)$$

with the GJ density given by

$$\rho_{GJ} = \frac{B_H \sqrt{A_H}}{4\pi \sqrt{-g}} \partial_\theta \left[\frac{\sin^2 \theta}{\alpha^2} (\omega - \Omega) \right]. \quad (7)$$

Note that $\Sigma \Delta \rho_{GJ}$ is finite on the horizon. Contours of $\rho_{GJ}(r, \theta)$ are exhibited in Figure 1 for $\Omega = 0.5\omega_H$

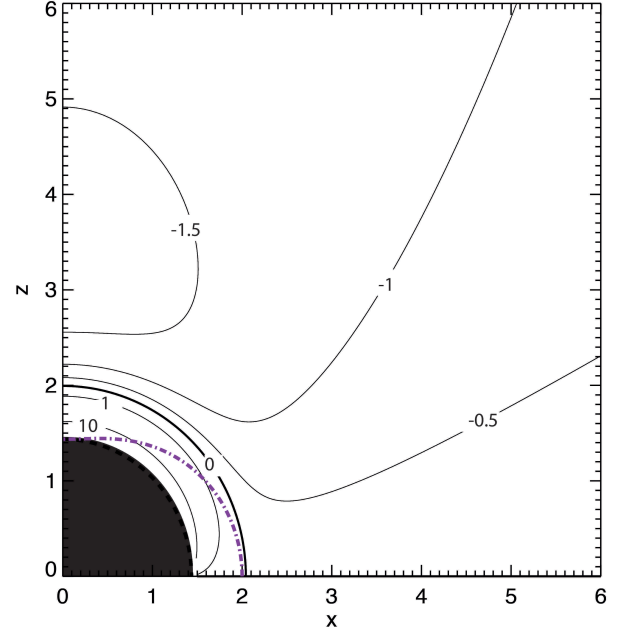


FIG. 1. Contours of the GJ charge density (solid lines), for $\tilde{a} = 0.9$, $\Omega = 0.5\omega_H$. The numbers that label the curves are values of $\rho_{GJ}(r, \theta)/\rho_0$, where ρ_0 is the fiducial value defined below Equation (7). The thick solid line corresponds to the null surface $r_c(\theta)$, on which $\rho_{GJ} = 0$. The black circle delineates the interior of the black hole, and the purple dashed-dotted line marks the static surface.

and $\tilde{a} = 0.9$. As seen, it vanishes on the null surface denoted here by $r_c(\theta)$, located roughly (but not exactly) where $\Omega = \omega$. In what follows the charge density and electric flux are normalized to the fiducial values $\rho_0 = B_H \omega_H \sqrt{A_H}/(2\pi c r_g^2) = B_H \tilde{a}/2\pi r_g$ and $\Phi_o = \rho_0 r_g^3$, respectively, densities are measured in units of $n_0 = \rho_0/e$, and angular velocities are measured in units of ω_H . With the convention $\mathbf{\Omega} \cdot \mathbf{B} > 0$ adopted below the electric field in the gap is negative, $\Phi_E < 0$.

C. Plasma dynamics

We adopt a treatment in which the plasma in the gap is modelled as a two-component fluid, consisting of electrons and positrons with proper number densities n_- and n_+ , respectively, and 4-velocities $u_\pm^\mu = (u_\pm^t, u_\pm^r, 0, 0)$. In a ZAMO frame the velocity components are given by $u_\pm = \sqrt{g_{rr}} u_\pm^r$, $\gamma_\pm = \alpha u_\pm^t$, $v_\pm = u_\pm/\gamma_\pm$. We define the radial fluxes, $N_\pm^r = \Sigma n_\pm u_\pm^r$, measured in units of $r_g^2 n_0 c$. The continuity equation for each species can then be expressed as (see appendix B),

$$\partial_\xi N_\pm^r = \frac{\Sigma \Delta}{2(r^2 + \tilde{a}^2)} Q, \quad (8)$$

where Q is the net pair production rate per unit volume, measured in units of $n_0 c/r_g$, and is the same for

electrons and positrons by virtue of charge conservation. It is readily seen that the difference $N_0^r = N_+^r - N_-^r$ is conserved along magnetic flux tubes. This conserved quantity is simply the electric current per solid angle per unit charge flowing along magnetic flux tube, viz., $N_0^r = \Sigma j^r / e$, where $j^r = e(n_+ u_+^r - n_- u_-^r)$ is the radial component of the electric 4-current density, which is determined by the global magnetospheric structure. The evaluation of N_0^r requires proper account of the coupling between the gap and the global magnetosphere, which is beyond the scope of our analysis, and in our model it is treated as a free parameter. As will be shown below, it affects the gap structure. The normalized charge density, $\rho_e = j^t / \rho_0 = e(n_+ u_+^t - n_- u_-^t) / \rho_0$, can be expressed in terms of the electron and positron fluxes as,

$$\rho_e = \frac{\sqrt{A}}{\Sigma \Delta} \left(\frac{N_+^r}{v_+} - \frac{N_-^r}{v_-} \right). \quad (9)$$

With the convention $\mathbf{\Omega} \cdot \mathbf{B} > 0$ ($\Phi_E < 0$) electrons accelerate outwards, $v_- > 0$, and positrons inwards, $v_+ < 0$. The equations of motion of the pair fluids can be expressed as (see appendix B for details),

$$\frac{d\gamma_{\pm}}{d\xi} = -\gamma_{\pm} \partial_{\xi} \ln \alpha \pm \frac{\alpha}{r^2 + \tilde{a}^2} \left(\eta_E \Phi_E - \sqrt{A} s_{\pm}^t \right), \quad (10)$$

with

$$\eta_E = \frac{e B_H \sqrt{A_H} \omega_H}{2\pi m_e c^3} = 1.4 \times 10^9 \tilde{a} B_8 m. \quad (11)$$

The first term on the right hand side of Equation (10) accounts for the gravitational redshift, the second term for energy gain due to acceleration in the gap electric field, and the third term for the sum of curvature and inverse Compton losses, $s_{\pm}^t = s_{\pm,cur}^t + s_{\pm,IC}^t$, derived explicitly below. As will be shown below, in practice the Lorentz factors γ_{\pm} equal their saturation values, at which energy gain is compensated by redshift effects and radiative losses almost everywhere in the gap.

D. Gamma-ray emission and pair production

We suppose that the gap is exposed to emission of soft photons by the accretion flow, from a putative source of size $R_s = \tilde{R}_s r_g$ and luminosity $L_s = l_s L_{Edd}$. For simplicity, we assume that the intensity of the seed radiation in the gap is isotropic with a power law spectrum: $I_s(x^\mu, \nu_s, \mathbf{\Omega}_s) = I_0(\epsilon_s / \epsilon_{s,min})^{-p}$, $\epsilon_{s,min} < \epsilon_s < \epsilon_{s,max}$, where $\epsilon_s = h\nu_s / m_e c^2$ is the dimensionless photon energy and $p > 1$. The assumption that I_s is isotropic is reasonable, except perhaps very near the horizon, since the size R_s of the radiation source is typically much larger than the gap dimensions. The number density of seed photons is given by

$$n_s = \frac{4\pi}{c} \int \frac{I_s}{h\nu_s} d\nu_s = \frac{4\pi I_0}{hc} \frac{(1 - \epsilon_{s,min}^p / \epsilon_{s,max}^p)}{p} \simeq \frac{4\pi I_0}{hc}. \quad (12)$$

We find it convenient to define a fiducial optical depth:

$$\tau_0 = \sigma_T r_g \frac{4\pi I_0}{hc} = A_s \frac{4m_p}{m_e} \frac{l_s}{\tilde{R}_s^2 \epsilon_{s,min}}, \quad (13)$$

where $A_s = (p-1)/[1 - (\epsilon_{s,min}/\epsilon_{s,max})^{p-1}] \sim 1$. It roughly gives the scaling of the IC and pair production opacities. Typically $\tilde{R} < 10^2$, so that a large opacity is anticipated when $l_s > \epsilon_{s,min}$.

As shown below, the terminal Lorentz factor of the pairs in the gap is extremely high. Thus, their emission is highly beamed along their direction of motion. Let $I_\gamma(r, \epsilon_\gamma, \mu_\gamma)$ denotes the intensity of gamma-rays emitted by the pairs at radius r , in direction $\mu_\gamma = \cos \theta_\gamma = \hat{r} \cdot \hat{\Omega}_\gamma$ and energy $\epsilon_\gamma = h\nu_\gamma / m_e c^2$. Under the beaming approximation we have:

$$I_\gamma(r, \epsilon_\gamma, \mu_\gamma) = I_\gamma^+(r, \epsilon_\gamma) \delta(\mu_\gamma + 1) + I_\gamma^-(r, \epsilon_\gamma) \delta(\mu_\gamma - 1), \quad (14)$$

here I_γ^- denotes the intensity emitted by electrons and I_γ^+ by positrons. The beamed intensities satisfy the radiative transfer equations

$$\frac{1}{\sqrt{A}} \frac{d}{d\xi} (\sqrt{A} I_\gamma^\pm) = \pm \frac{\alpha \sqrt{A}}{r^2 + \tilde{a}^2} (\kappa_{pp} I_\gamma^\pm - j_\gamma^\pm), \quad (15)$$

neglecting redshift effects (see appendix C for details), where the emissivity is the sum of curvature and IC emissions, $j_\gamma^\pm = j_{IC}^\pm + j_{cur}^\pm$. The absorption coefficient κ_{pp} and the emissivities j_{IC}^\pm and j_{cur}^\pm are computed in the ZAMO frame. To render this equation dimensionless, we normalize intensities by hcn_0 , emissivities by hcn_0/r_g , and opacities by $1/r_g$.

1. Curvature emission

The normalized curvature emissivity is given by [22]

$$j_{cur}^\pm(r, \epsilon_\gamma) = \frac{\sqrt{3} \alpha_f n_{\pm} \gamma_{\pm}^2}{2\pi R_c} F(\epsilon/\epsilon_c), \quad (16)$$

where R_c denotes the curvature radius of magnetic field lines (in units of r_g), $\alpha_f = e^2/\hbar c$ is the fine structure constant, $F(x)$ is the usual synchrotron function, and

$$\epsilon_c = \frac{2\pi \lambda_c}{r_g} \frac{\gamma_{\pm}^3}{R_c} \simeq 10^{-15} \frac{\gamma_{\pm}^3}{m R_c}, \quad (17)$$

here $\lambda_c = \hbar/m_e c$ denotes the Compton wavelength of the electron. The curvature radius is a free parameter in our model. In the numerical calculations presented below we adopted $R_c = 1$. Finally, the curvature loss term is given by

$$s_{\pm,cur}^t = -10^{-18} \frac{\gamma_{\pm}^4}{m R_c^2}. \quad (18)$$

2. Inverse Compton emission

The normalized IC emissivity, computed in appendix C using the full Klein-Nishina (KN) cross-section, can be expressed in the ZAMO frame in terms of the fiducial optical depth τ_0 as:

$$j_{IC}^{\pm}(r, \epsilon_{\gamma}) = \frac{\tau_0 n_{\pm} \gamma_{\pm}}{6\pi} \left[\frac{4\gamma_{\pm} \epsilon_{s,min} (\gamma_{\pm} - \epsilon_{\gamma})}{\epsilon_{\gamma} + 4\gamma_{\pm} \epsilon_{s,min} (\gamma_{\pm} - \epsilon_{\gamma})} \right]^p \times \left[\frac{\epsilon_{\gamma}}{\epsilon_{\gamma} + 4\gamma_{\pm} \epsilon_{s,min} (\gamma_{\pm} - \epsilon_{\gamma})} \right]. \quad (19)$$

The corresponding drag (energy loss) terms for the pairs are given formally by

$$s_{\pm, IC}^t(r) = -\frac{2\pi}{n_{\pm} \gamma_{\pm}} \int_0^{\gamma_{\pm}} j_{IC}^{\pm}(r, \epsilon_{\gamma}) d\epsilon_{\gamma}. \quad (20)$$

Within the beaming approximation invoked here, transition from the Thomson to the KN regime occurs at a Lorentz factor $\gamma_{KN} = 1/4\epsilon_{s,min}$. In the Thomson limit, where $\gamma/\gamma_{KN} = 4\gamma_{\pm} \epsilon_{s,min} \ll 1$, the above expressions reduce to

$$j_{IC}^{\pm}(r, \epsilon_{\gamma}) \simeq \frac{\tau_0 n_{\pm} \gamma_{\pm}}{6\pi} \left(\frac{\epsilon_{\gamma}}{4\gamma_{\pm}^2 \epsilon_{s,min}} \right)^{-p}, \quad (21)$$

with $4\gamma_{\pm}^2 \epsilon_{s,min} \leq \epsilon_{\gamma}$, and

$$s_{\pm, IC}^t(r) \simeq -\frac{4\tau_0}{3(p-1)} \gamma_{\pm}^2 \epsilon_{s,min}, \quad (22)$$

whereas in the KN limit, $\gamma_{\pm}/\gamma_{KN} \gg 1$, we have

$$j_{IC}^{\pm}(r, \epsilon_{\gamma}) \simeq \frac{\tau_0 n_{\pm} \gamma_{\pm}}{6\pi} \left(\frac{\epsilon_{\gamma}}{4\gamma_{\pm}^2 \epsilon_{s,min}} \right), \quad (23)$$

and

$$s_{\pm, IC}^t(r) \simeq -\frac{\tau_0}{24 \epsilon_{s,min}}. \quad (24)$$

3. Pair production

Under the assumption that the seed photon intensity is isotropic, the normalized pair production opacity simplifies to

$$\kappa_{pp}(r, \epsilon_{\gamma}) = \frac{\tau_0}{2} \int_{\epsilon_{th}}^{\epsilon_{s,max}} d\ln \epsilon_s \left(\frac{\epsilon_s}{\epsilon_{s,min}} \right)^{-p} \times \int_{-1}^{\mu_{max}} d\mu (1 - \mu) \sigma_{\gamma\gamma} \quad (25)$$

where $\sigma_{\gamma\gamma}$ is the full pair creation cross-section (in units of σ_T) given in Ref [23], $\epsilon_{th} = \max(\epsilon_{s,min}, \epsilon_{\gamma}^{-1})$ and $\mu_{max} = 1 - 2/(\epsilon_s \epsilon_{\gamma})$ from the threshold condition. In the Thomson limit, that is, $\epsilon_{\gamma} \epsilon_{s,min} < 1$, it is given, to a good approximation, by [21]

$$\kappa_{pp}(r, \epsilon_{\gamma}) = \frac{3\tau_0}{2} A_p(\epsilon_{s,min} \epsilon_{\gamma})^p, \quad (26)$$

where A_p is a number that depends on the spectral index p , and is plotted in Figure 1 of Ref [21]. It equals roughly 0.2 for $p = 1$ and 0.1 for $p = 2$. In the KN limit, $\epsilon_{\gamma} \epsilon_{s,min} \gg 1$, we can use the approximation $\int_{-1}^{\mu_{max}} (1 - \mu) \sigma_{\gamma\gamma} d\mu \simeq 3 \ln(\epsilon_{\gamma} \epsilon_s) / 2 \epsilon_{\gamma} \epsilon_s$, to obtain

$$\kappa_{pp}(r, \epsilon_{\gamma}) = \frac{3\tau_0}{4(p+1)} \frac{\ln(\epsilon_{\gamma} \epsilon_{s,min})}{\epsilon_{\gamma} \epsilon_{s,min}}. \quad (27)$$

For the parameter regime considered here we find $\ln(\epsilon_{\gamma} \epsilon_{s,min}) / 2(p+1) \simeq 1$. Thus, to a good approximation we can use the simple extrapolation:

$$\kappa_{pp}(r, \epsilon_{\gamma}) = \frac{3\tau_0}{2} \frac{A_p(\epsilon_{s,min} \epsilon_{\gamma})^p}{1 + A_p(\epsilon_{s,min} \epsilon_{\gamma})^{p+1}}. \quad (28)$$

The net specific pair production rate can be expressed as

$$Q = 2\pi \int d\ln \epsilon_{\gamma} \int_{-1}^1 d\mu \kappa_{pp} I_{\gamma}(r, \epsilon_{\gamma}, \mu_{\gamma}) \quad (29)$$

$$= 3\pi\tau_0 \int \frac{A_p(\epsilon_{\gamma} \epsilon_{s,min})^p}{1 + A_p(\epsilon_{\gamma} \epsilon_{s,min})^{p+1}} (I_{\gamma}^+ + I_{\gamma}^-) d\ln \epsilon_{\gamma}.$$

E. Boundary conditions

The outer and inner gap boundaries are treated as free boundaries. Their location is determined by two parameters; the global current N_0^r and the fiducial optical depth τ_0 . In the steady gap model it is implicitly assumed that beyond the gap boundaries the field aligned electric field vanishes. Thus, it must satisfy the boundary conditions

$$\Phi_E(r_{in}) = \Phi_E(r_{out}) = 0. \quad (30)$$

We further assume that pairs and photons are not injected into the gap across either boundary. This implies

$$N_+^r(r_{out}) = N_-^r(r_{in}) = 0, \quad N_-^r(r_{out}) = -N_+^r(r_{in}) = -N_0^r. \quad (31)$$

Likewise, since no gamma-rays are incident into the gap through its boundaries,

$$I_{\gamma}^+(r_{out}, \epsilon_{\gamma}) = I_{\gamma}^-(r_{in}, \epsilon_{\gamma}) = 0. \quad (32)$$

The Lorentz factors of the electron and positron beams formally satisfy $\gamma_-(r_{in}) = \gamma_+(r_{out}) = 1$. However, since practically they reach their saturation level instantaneously, we find that the solution is highly insensitive to the exact values taken at the boundary, as long as they are much smaller than the maximum values.

IV. STEADY GAP SOLUTIONS AND FORBIDDEN REGIMES

Equations (6)-(10), (15), (16), (19), (28) and (29), subject to the boundary conditions (30)-(32) form a complete

set that governs the structure and spectrum of the steady gap for a given choice of the input parameters N_0^r and τ_0 (if a solution exists). The location of the outer boundary r_{out} is constrained to exceed a minimum value by the condition $|\rho_e(r_{out})| < |\rho_{GJ}(r_{out})|$. To obtain a solution, we integrate the equations iteratively, changing the locations of the inner and outer boundaries, r_{in} and r_{out} , in each iteration, until all boundary conditions are satisfied. In each iteration we first guess a value for r_{out} , and then integrate the equations inwards starting at r_{out} until Φ_E vanishes (provided it is outside the horizon). We then check the values of N_-^r and I_γ^- there, and if nonzero change the location of r_{out} accordingly for the next iteration. The process is repeated until the desired solution is obtained.

Examples are exhibited in Figure 2, where profiles of the electric flux, Lorentz factor, pair fluxes and specific pair production rate, computed for a prototypical supermassive BH accreting in the RIAF regime ($\dot{m} \simeq 10^{-4}$), are plotted for different values of the magnetospheric current, here represented in terms of the current density at the null surface, $j_c = eN_0^r/\Sigma_c$ (normalized by the fiducial current $\Omega B_H \cos \theta/2\pi$), where $\Sigma_c \equiv \Sigma(r_c)$ is the value of $\Sigma(r)$ at the null surface $r_c(\theta)$. Each case shown corresponds to a specific value of τ_0 . Similar solutions were obtained for parameters typical to stellar BHs. As seen, the gap shrinks as the magnetospheric current j_c (or equivalently the flux N_0^r) is reduced, as expected. It is also seen that unless the magnetospheric current is unlikely weak, the gap width is not much smaller than the horizon scale. Since in a stationary gap the pair multiplicity cannot largely exceed unity (see bottom right panel in Fig. 2), this implies that τ_0 (and hence L_s) must also be small, as shown next.

Much insight can be gained into the behaviour of the gap by employing crude estimates that allow analytic derivation of the pair production rate and the closure condition. Below, we adopt such a treatment to map the parameter regime in which local, steady gap solutions exist.

The Lorentz factor of accelerating pairs is limited by the saturation value at which the radiation drag (due to curvature and IC emission) balances the electric force acting on the particles within the gap. It formally obtained by setting the right hand side of Eq. (10) to zero. Neglecting gravity (which is important only very near the horizon) we find that the acceleration length is roughly $l_{acc} \simeq 10^{-2} m^{-1/2} R_c^{1/2} (B_8 |E_r'|)^{-3/4}$, so that practically the Lorentz factor is determined by the saturation condition in the entire gap region. The dependence of γ/γ_{KN} , the saturated Lorentz factor normalized by $\gamma_{KN} \equiv 1/4\epsilon_{s,min}$, on τ_0 is displayed in Fig 3, for different values of the peak energy ϵ_{min} . The transition from curvature dominated to IC dominated losses is clearly seen. The value of τ_0 at which the transition occurs depends on the spectral peak ϵ_{min} through Klein-Nishina effects. It can be estimated analytically from the saturation condition, whereby it is found that IC losses dominate the

drag force when $\tau_0 > 10^4 B_8 m (\epsilon_{s,min}/10^{-6})$, as indeed seen in Figure 3. As argued below, for such high values of τ_0 steady gap solutions do not exist for any reasonable choice of parameters, hence this regime is irrelevant for our analysis. At smaller values of τ_0 curvature losses dominate, and the saturated Lorentz factor is:

$$\gamma_{\pm} \simeq 5 \times 10^6 R_c^{1/4} (B_8 |E_r'|)^{1/4} m^{1/2}, \quad (33)$$

so that $\gamma_+ = \gamma_- = \gamma$. Under a broad range of conditions we find $|E_r'|^{1/4} \sim 1$. Hence, for our fiducial stellar black hole, $m = 10$, $B_8 = 1$, we expect $\gamma \sim 10^7$, whereas for a fiducial blazar with $m = 10^9$ and $B_8 = 10^{-4}$ we have $\gamma \simeq 10^{10}$. Our detailed calculations confirm this. Under our beaming approximation, IC scattering is in the KN limit if (see Eq. 19)

$$\epsilon_{s,min} > \frac{1}{4\gamma} \simeq 5 \times 10^{-8} R_c^{-1/4} (B_8 |E_r'|)^{-1/4} m^{-1/2}. \quad (34)$$

This condition is satisfied essentially in all sources. Consequently, we conclude that quite generally IC scattering of external radiation by pairs accelerated in the gap is in the KN regime (although sufficiently soft extension of the spectrum to energies below the peak may somewhat alter this conclusion). The characteristic energy of curvature photons, Equation (17), can be expressed as

$$\epsilon_c \simeq 10^5 (B_8 |E_r'|)^{3/4} R_c^{-1/4} m^{1/2}, \quad (35)$$

and it is seen that typically $\epsilon_c \ll \gamma$. Consequently, we expect two peaks in the high-energy spectrum emitted from the gap, one due to IC scattering, at $\epsilon_\gamma \simeq \gamma$, and the other one due to curvature emission, at $\epsilon_\gamma \simeq 0.3\epsilon_c$. Equations (33) and (35) imply that the separation between the peaks is independent of the black hole mass, but scales with the magnetic field roughly as $B^{1/2}$. The detailed calculations outlined in Ref [6] indeed confirm that the spectral energy distribution has a double peak structure with these scalings.

Next, we provide estimates for the pair production opacity and the specific pair production rate in the gap. Since IC scattering is in the KN regime, the characteristic energy of scattered photons is γ . Thus, pair creation occurs also in the KN regime, whereby Equation (27) applies:

$$\begin{aligned} \kappa_{pp,IC} &= \frac{3\tau_0}{4(p+1)} \frac{\ln(\gamma\epsilon_{s,min})}{\gamma\epsilon_{s,min}} \sim 0.1\tau_0 R_c^{-1/4} \quad (36) \\ &\times (B_8 |E_r'|)^{-1/4} m^{-1/2} \left(\frac{\epsilon_{s,min}}{10^{-6}} \right)^{-1}, \end{aligned}$$

for $p > 1$. Consequently, for $\tau_0 > 10 R_c^{1/4}$, $\kappa_{pp,IC} \gtrsim 1$ for both stellar and supermassive black holes. At these energies the contribution of curvature emission is completely negligible (see Eq. (35)), and the solution to the radiative transfer equation, Eq. (15), is approximately the IC source function, specifically $I_\gamma^\pm \simeq j_{IC}^\pm/\kappa_{pp}$. Using Equation (29) and noting that in the ultra-relativistic limit

$n_+\gamma_+ + n_-\gamma_- = -N_0^r/\sqrt{\Sigma\Delta}$, one obtains the contribution of IC scattered photons to the pair creation rate:

$$Q_{IC}(r) \simeq \frac{\tau_0}{12\gamma\epsilon_{min}} \frac{(-N_0^r)}{\sqrt{\Sigma\Delta}} \simeq 0.02\tau_0 \frac{(-N_0^r)}{\sqrt{\Sigma\Delta}} \quad (37)$$

$$\times R_c^{-1/4} (B_8|E'_r|)^{-1/4} m^{-1/2} \left(\frac{\epsilon_{s,min}}{10^{-6}}\right)^{-1}.$$

The peak of curvature emission occurs at an energy of $\epsilon_\gamma = 0.29\epsilon_c$, for which $\epsilon_\gamma\epsilon_{s,min} \ll 1$. Thus, the interaction of curvature photons with the target radiation field is in the Thomson regime. Choosing $p = 2$ for illustration, Equation (26) yields

$$\kappa_{pp,cur}(\epsilon_\gamma) \simeq 10^{-4} \tau_0 m R_c^{-1/2} (B_8|E'_r|)^{3/2} \quad (38)$$

$$\times \left(\frac{\epsilon_{s,min}}{10^{-6}}\right)^2 \left(\frac{\epsilon_\gamma}{0.29\epsilon_c}\right)^2$$

at energies $\epsilon_\gamma \lesssim \epsilon_c$. Since for a steady gap $\tau_0 \ll 10^4$, it implies $\kappa_{pp,cur} \ll 1$. The calculation of Q_{cur} is more involved than in the IC case, and we can only offer a rough analytic estimate of its average. The details can be found in appendix D, where the following result for the average pair production rate is derived:

$$\langle Q_{cur} \rangle \simeq 2 \tau_0 (-N_0^r) R_c^{-5/4} (B_8|E'_r|)^{7/4} \quad (39)$$

$$\times m^{3/2} \left(\frac{\epsilon_{s,min}}{10^{-6}}\right)^2 \frac{1}{\langle \sqrt{A} \rangle} \int_{r_{in}}^{r_{out}} \frac{\sqrt{A} dr}{\Delta},$$

here $\langle \sqrt{A} \rangle$ is the average value of $\sqrt{A(r)}$ across the gap, defined explicitly below Equation (D2), and is typically in the range 3 to 4.5. Equation (39) may overestimate the local rate by a factor of a few. From a comparison of Eqs. (37) and (39) we anticipate the pair production to be dominated by IC photons when $B_8 \lesssim 0.1m^{-1}(\epsilon_{min}/10^{-6})^{-3/2}R_c$. This condition is roughly satisfied in RIAF sources with $\dot{m} < 10^{-4}$, assuming $R_c \simeq 1$. At larger accretion rates pair production is predominantly due curvature photons.

Finally, we derive a closure condition that defines a limit on the luminosity of the external radiation source, l_s , above which steady gap solutions are forbidden. For clarity of our analysis we include only the contribution of IC photons to the pair production rate, viz., $Q = Q_{IC}$. Thus, the limit obtained from the closure condition derived below should be considered an absolute upper limit. Additional production of pairs by curvature photons would merely enlarge the forbidden regime. Integration of Equation (8), subject to the boundary condition $N_+^r(r_{out}) = 0$, yields $N_0^r = \int_{r_{in}}^{r_{out}} (\Sigma Q/2) dr$. This last relation simply means that the pair multiplicity in the gap is roughly unity. Taking $Q = Q_{IC}$ in the latter expression and substituting Eq. (37) yields

$$\tau_0 = \frac{12\gamma\epsilon_{min}}{H} \simeq 50 \frac{(R_c B_8 |E'_r|)^{1/4} m^{1/2} (\epsilon_{min}/10^{-6})}{H}, \quad (40)$$

where the factor $H = \int_{r_{in}}^{r_{out}} \sqrt{\Sigma/\Delta} dr$ depends on the magnetospheric current N_0^r through the gap boundaries

r_{in} and r_{out} , and is of order a few for the solutions shown in Figure 2. It can become much smaller than unity for extremely small values of N_0^r , but we find such values unlikely. For our fiducial sources the value of $B_8^{1/4} m^{1/2} (\epsilon_{min}/10^{-6})$ is about 3 in case of a stellar BH and about 30 for a supermassive BH. The maximum value of $|E'_r|^{1/4}$ ranges between 0.8 and 1.3 in the solutions exhibited in Figure 2. Consequently, the corresponding Eddington ratio, $l_s = 1.3 \times 10^{-7} (\dot{R}_s/30)^2 (\epsilon_{min}/10^{-6}) \tau_0$ (see Eq. (13)), that allows stationary gap solutions must be very small. Larger values would render the gap intermittent.

Figure 4 shows the separation into forbidden and allowed regimes computed numerically using the full gap equations with $Q = Q_{IC}$. The solid curve corresponds to the locus of solutions, each having the maximum value of τ_0 above which no steady solutions exist. For each choice of the magnetospheric current N_0^r this maximum value is obtained by seeking the solution that satisfies $\rho_e(r_{out}) = \rho_{GJ}(r_{out})$, or equivalently $\sqrt{A(r_{out})} [\alpha(r_{out})]^2 \rho_{GJ}(r_{out}) = N_0^r$. This solution defines the maximum luminosity l_s at which a steady gap can still support the current N_0^r . At lower luminosities the gap widens (r_{out} increases). At larger luminosities it must become intermittent.

V. A REMARK ON THE GLOBAL STRUCTURE

In this section we briefly comment on the relation between the local gap and the global magnetospheric structure. As mentioned above, a generic feature of magnetically driven outflows from a Kerr black hole is a plasma double-flow that emanates from a stagnation surface located between the inner and outer Alfvén surfaces. The location of the stagnation surface is determined from a balance between the gravitational, centrifugal and Lorentz forces [26]. In the limit of low inertia considered in this paper (where a gap forms) it depends very weakly on the details of plasma injection [18]. In general, it has a non-spherical shape [11, 18], and its distance from the BH ranges from $r \sim 4.5r_g$ in the equator to $r \sim 10r_g$ along the axis, so that it is located well outside the null surface (see Figure 5 for illustration). Now, if the outer gap boundary extends beyond the stagnation surface, then accelerated particles leaving the outer gap boundary move outwards and particles the escape through the inner gap boundary move inwards, in accord with the global plasma flow requirements. On the other hand, if the outer gap boundary lies below the stagnation surface, then the direction of the particle beam that escapes through the outer gap boundary is opposite to that of the plasma flow in the force-free section below the stagnation surface, as illustrated schematically in Figure 5. This inconsistency most likely means that the plasma production process must be dynamic. As seen in Figure 2, in all steady solutions the outer gap boundary does

not extend beyond $3r_g$, so that it is located below the stagnation surface. This suggests that the local steady solutions derived here may be inapplicable to a global magnetosphere.

VI. CONCLUSIONS

The main conclusion of this paper is that under realistic conditions, charge-starved regions in the magnetosphere of a Kerr black hole are expected to be inherently intermittent. The main reasons are that (i) for realistic values of the magnetospheric current the pair multiplicity cannot accommodate the closure condition required by a steady gap, unless the luminosity of the external radiation source is extremely small, and (ii) the steady gap solutions are inconsistent with the global magnetospheric structure. The latter reason seems to imply that in black hole outflows the entire region below the stagnation surface should be dynamic. It is unclear at present how the intermittency of the plasma production process will affect the resultant emission. In local gap models the plasma production process can be sporadic, giving

rise to electric current oscillations around the mean value imposed by the global magnetosphere with an amplitude that depends on the pair production rate. In this case, a reduction in the amplitude of the gap oscillations is expected when the intensity of the ambient radiation field, that provides the dominant pair production opacity, is increased. In global, self-consistent gap models it seems that plasma production should occur in cycles of pair creation bursts. What is the fraction of the black hole spin down power that can be released in the form of high-energy radiation in this dynamic state and how this should affect the emitted spectrum is yet an open question.

Intermittency is expected also in pulsar gaps under certain conditions [27, 28], however, the reason for this is different than in the case of rotating black holes discussed here.

ACKNOWLEDGMENTS

This research was supported by a grant from the Israel Science Foundation no. 1277/13.

Appendix A: Derivation of the generalized Gauss' law

From the inhomogeneous Maxwell's equations,

$$\frac{1}{\sqrt{-g}}\partial_\mu(\sqrt{-g}F^{\nu\mu}) = 4\pi j^\nu, \quad (\text{A1})$$

and the relation

$$F^{t\mu} = g^{\mu\nu}(g^{tt}F_{t\nu} + g^{t\varphi}F_{\varphi\nu}) = \frac{1}{\alpha^2}g^{\mu\nu}(F_{\nu t} + \omega F_{\nu\varphi}) \quad (\text{A2})$$

one obtains the generalized Gauss' law:

$$\frac{1}{\sqrt{-g}}\partial_\mu \left[\frac{\sqrt{-g}g^{\mu\nu}}{\alpha^2}(F_{\nu t} + \omega F_{\nu\varphi}) \right] = 4\pi j^t. \quad (\text{A3})$$

In terms of the electric field measured in a frame rotating with the flux tube,

$$F'_{\alpha t} = F_{\alpha t} + \Omega F_{\alpha\varphi}, \quad (\text{A4})$$

the latter equation can be written as

$$\frac{1}{\sqrt{-g}}\partial_\mu \left[\frac{\sqrt{-g}g^{\mu\nu}}{\alpha^2}F'_{\nu t} \right] = 4\pi(j^t - \rho_{GJ}), \quad (\text{A5})$$

where

$$\rho_{GJ} = \frac{1}{4\pi\sqrt{-g}}\partial_\mu \left[\frac{\sqrt{-g}g^{\mu\nu}}{\alpha^2}(\omega - \Omega)F_{\nu\varphi} \right]. \quad (\text{A6})$$

For the static, axisymmetric radial gap invoked in section III we have $\partial_t = \partial_\varphi = 0$ and $F'_{\theta t} = 0$, whereby the expression for ρ_{GJ} reduces to Equation (7), and Equation (A5) reduces to

$$\frac{1}{\Sigma}\partial_r \left(\frac{A}{\Sigma}F'_{rt} \right) = 4\pi(j^t - \rho_{GJ}), \quad (\text{A7})$$

where the substitutions $\sqrt{-g} = \Sigma \sin \theta$ and $\sqrt{-g}g^{rr}/\alpha^2 = (A/\Sigma) \sin \theta$ have been used. Upon defining the electric flux as $\Phi_E = AF'_{rt}/\Sigma$ and transforming to the tortoise coordinate given in Equation (5), Equation (6) is obtained.

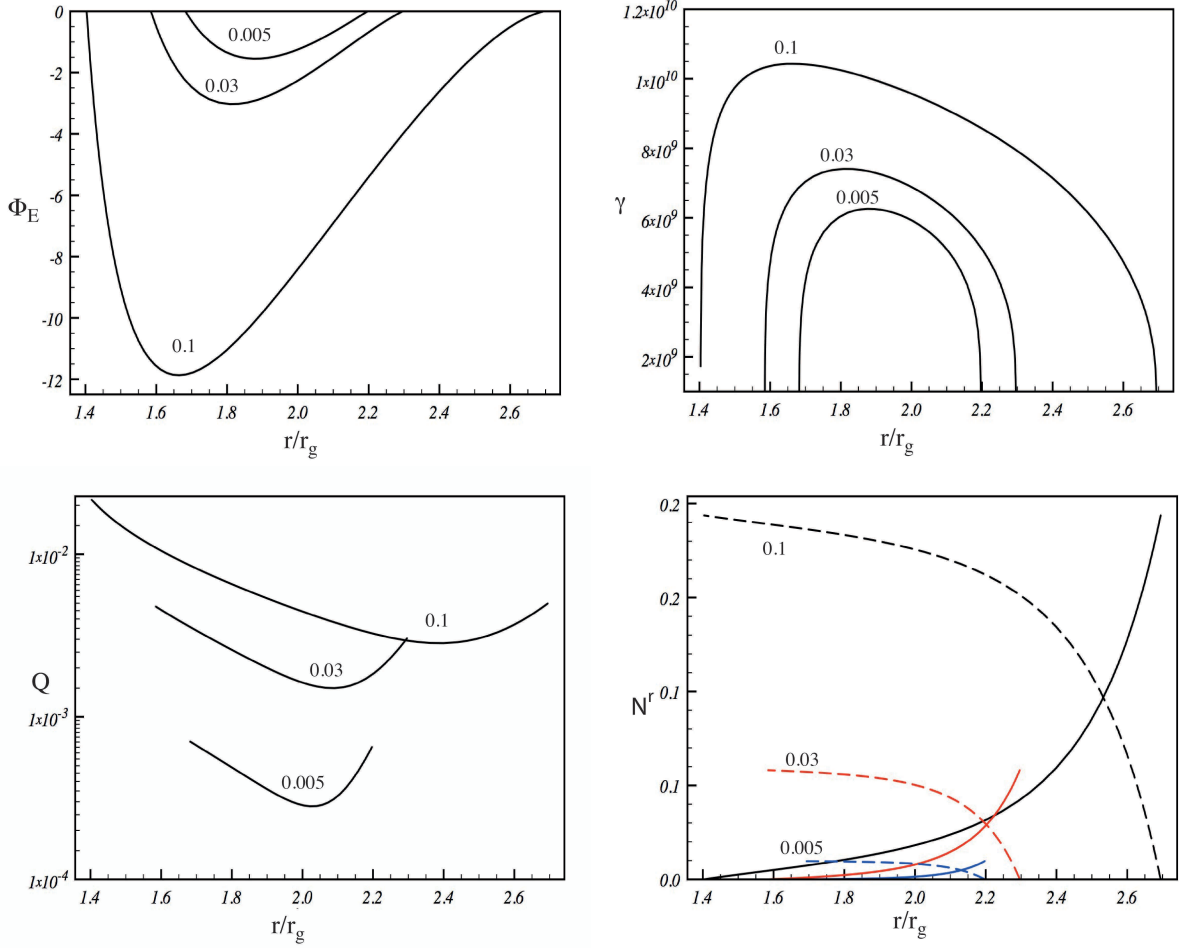


FIG. 2. Solutions of a steady gap for different values of the normalized magnetospheric current, $2\pi j_c^r/(\Omega B_H \cos \theta)$ (indicated by the numbers that label the curves). The parameters used in all cases shown are $\theta = 30^\circ$, $M = 10^9 M_\odot$, $B_8 = 10^{-6}$, $\epsilon_{s,min} = 10^{-8}$. Shown are the profiles of the electric flux (upper left panel), Lorentz factor of the pairs (upper right panel), pair creation rate (lower left panel) and particle fluxes (lower right panel). The solid lines in the lower right panel correspond to the electron flux N_-^r and the dashed lines to the positron flux N_+^r .

Appendix B: Derivation of the fluid equations

The plasma in the gap is treated as a two-component fluid consisting of electrons and positrons, with proper densities n_\pm , pressures p_\pm , specific enthalpies (per particle) h_\pm , and 4-velocities u_\pm^μ , where subscript $-$ ($+$) designates the electron (positron) fluid. In the presence of pair creation the continuity equation becomes,

$$\frac{1}{\sqrt{-g}} \partial_\mu (\sqrt{-g} n_\pm u_\pm^\mu) = Q/2, \quad (\text{B1})$$

here Q denotes the pair production rate per unit volume. The electric 4-current is given by

$$j^\mu = e(n_+ u_+^\mu - n_- u_-^\mu), \quad (\text{B2})$$

and from Eq. (B1) it is readily seen that the electric current is conserved, viz., $\partial_\mu j^\mu = 0$. In a steady gap this implies that the current is constant inside the gap, $\nabla \cdot \mathbf{j} = 0$.

The energy-momentum equation takes the form:

$$\frac{1}{\sqrt{-g}} \partial_\nu (\sqrt{-g} T_\pm^{\mu\nu}) + \Gamma^\mu_{\alpha\beta} T_\pm^{\alpha\beta} = \pm e n_\pm F^\mu{}_\alpha u_\pm^\alpha - S_\pm^\mu + Q_\pm^\mu, \quad (\text{B3})$$

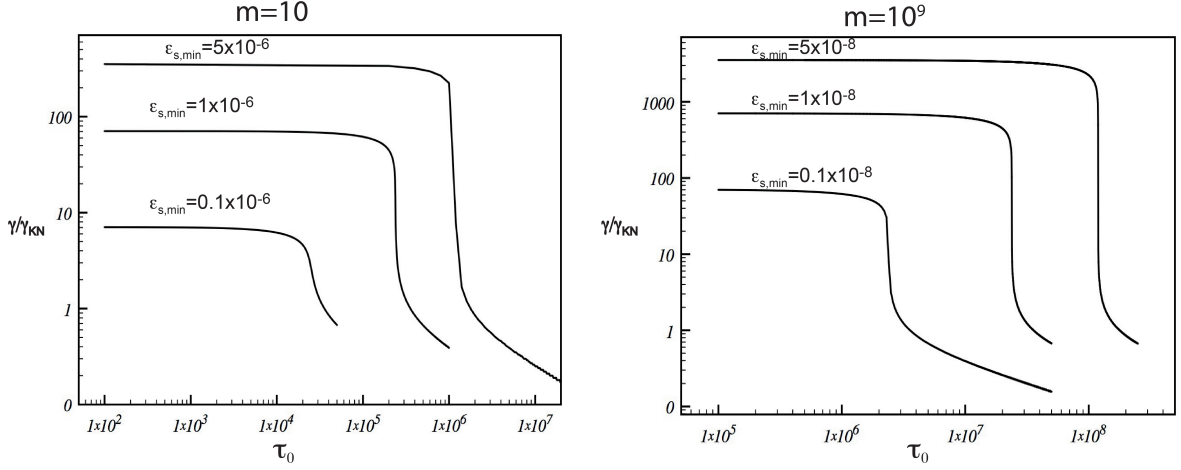


FIG. 3. Dependence of the terminal Lorentz factor γ (normalized to $\gamma_{KN} = 1/4\epsilon_{s,min}$) on the fiducial depth τ_0 , for different values of $\epsilon_{s,min}$ (indicated by the numbers that label the curves). The left panel corresponds to a stellar black hole with $m = 10$ and $B_8 = 1$, and the right panel to a supermassive black hole with $m = 10^9$ and $B_8 = 10^{-4}$. The sharp decline delineates the transition from curvature dominated to IC dominated drag.

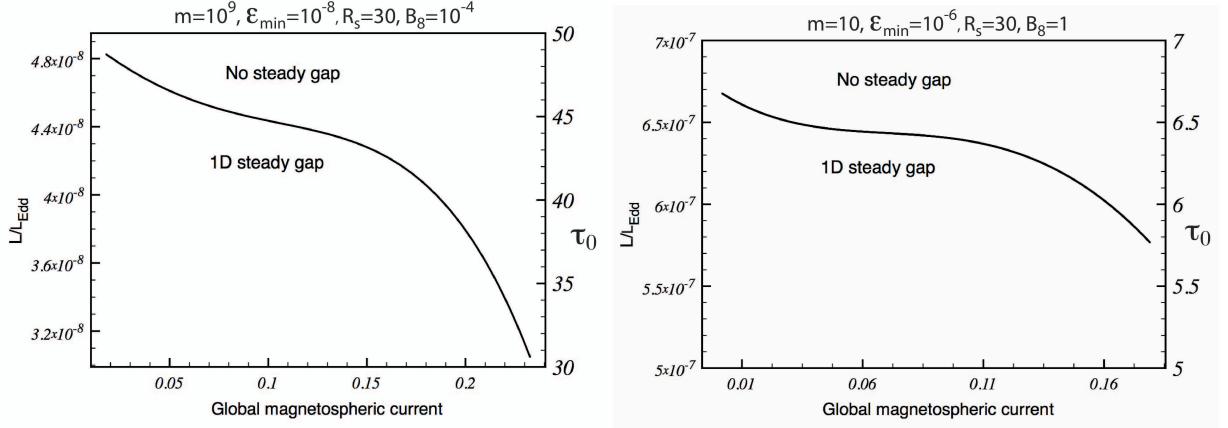


FIG. 4. Maximum Eddington ratio below which local steady gap solutions exist, versus normalized magnetospheric current, $2\pi j_c^r/(\Omega B_H \cos \theta)$, for two fiducial sources, stellar BH and supermassive BH, characterized by the parameters indicated in the figure label. The right axis shows the corresponding value of τ_0 .

in terms of the energy-momentum tensor

$$T_{\pm}^{\mu\nu} = h_{\pm} n_{\pm} u_{\pm}^{\mu} u_{\pm}^{\nu} + p_{\pm} g^{\mu\nu}. \quad (B4)$$

The first term on the right hand side of Eq. (B3) accounts for the work done on the fluids by electromagnetic forces, the second term (S_{\pm}^{μ}) for radiative losses, and the third term (Q_{\pm}^{μ}) is associated with pair loading via annihilation of photons. The projection of Eq. (B3) on the 4-velocity u^{ν} yields an equation for the change in the entropy per particle σ (in k_B units) of each fluid:

$$n_{\pm} T_{\pm} u_{\pm}^{\mu} \nabla_{\mu} \sigma_{\pm} = (S_{\pm\alpha} - Q_{\pm\alpha}) u_{\pm}^{\alpha} - h_{\pm} Q/2, \quad (B5)$$

here T_{\pm} is the temperature of the fluids. By employing Eqs. (B1), (B3)-(B5), and the second law, $dh - dp/n = Td\sigma$, we arrive at

$$n_{\pm} h_{\pm} u_{\pm}^{\mu} \nabla_{\mu} u_{\pm}^{\nu} = \pm e n_{\pm} F_{\alpha}^{\nu} u_{\pm}^{\alpha} + (-S_{\pm\alpha} + Q_{\pm\alpha} - \partial_{\alpha} p_{\pm})(g^{\alpha\nu} + u_{\pm}^{\alpha} u_{\pm}^{\nu}), \quad (B6)$$

denoting $u_{\pm}^{\mu} \nabla_{\mu} u_{\pm}^{\nu} = u_{\pm}^{\mu} \partial_{\mu} u_{\pm}^{\nu} + \Gamma_{\alpha\beta}^{\nu} u_{\pm}^{\alpha} u_{\pm}^{\beta}$. We now make the following approximations: First, pressure forces are expected to be small compared with the electric and radiation forces, thus we neglect the term $\partial_{\alpha} p_{\pm}$. Second, we

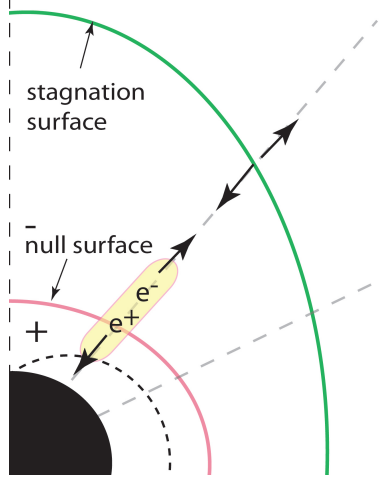


FIG. 5. A sketch of the global structure. The gap is represented by the yellowish stripe. The thick arrows point to the direction of the electron (positron) beam leaving the outer (inner) gap boundary. The two arrows that emanate from the stagnation surface show the flow directions of the plasma in the force-free region.

assume that each fluid is approximately adiabatic, $u^\nu \nabla_\nu \sigma_\pm = 0$. This assumption is reasonable if the spread in momentum is much smaller than the bulk momentum. Under the above simplifications Eq. (B5) yields $(-S_{\pm\alpha} + Q_{\pm\alpha} - \partial_\alpha p_\pm)(g^{\alpha\nu} + u_\pm^\nu u_\pm^\nu) = -S_\pm^\nu + Q_\pm^\nu - Q h u_\pm^\nu / 2$. Third, if newly created pairs are added to the fluid with an average momentum that is roughly equal to the bulk momentum (as naively expected from energy-momentum conservation), then $Q_\pm^\nu - Q h u_\pm^\nu / 2 = 0$. With these approximations the radiative source term is orthogonal to the fluid velocity, viz., $u_\pm^\nu S_{\pm\nu} = 0$.

Next, we take the radial ($\nu = r$) component of Eq. (B6), make use of the relation $u_\pm^\mu \nabla_\mu u_{\pm r} = u_\pm^\mu \partial_\mu u_{\pm r} - \Gamma_{\alpha r \beta} u_\pm^\alpha u_\pm^\beta$ and the fact that $u_r \Gamma_{\alpha\beta}^r = u^r \Gamma_{r\alpha\beta}$, and note that for the invoked gap geometry $u^\mu \partial_\mu = u^r \partial_r$, to get

$$\partial_r(u_\pm^2/2) = \frac{1}{2}(u_r \partial_r u^r + u^r \partial_r u_r) = -\frac{1}{2}(u_\pm^t)^2 \partial_r \alpha^2 \pm \frac{e}{h_\pm} F_{rt} u_\pm^t + s_{\pm r} u_\pm^t, \quad (\text{B7})$$

where $s_\pm^r = -S_\pm^r / (u_\pm^t n_\pm h_\pm)$ and $s_{\pm r} = g_{rr} s_\pm^r$. Noting that ∂_φ is a Killing vector we further have

$$-u^\mu \nabla_\mu u_{\pm\varphi} = \pm \frac{e}{n_\pm h_\pm} F_{\varphi\nu} u^\nu + s_{\pm\varphi} = s_{\pm\varphi}, \quad (\text{B8})$$

since $F_{\varphi\nu} u^\nu = F_{\varphi r} u^r = 0$ for the split monopole geometry invoked in our gap model. Neglecting the toroidal component of the radiative force, $s_{\pm\varphi} = 0$, which is reasonable for the assumed isotropic radiation field, implies that the angular momentum of each fluid is conserved: $u_{\pm\varphi} = g_{\varphi\varphi}(u^\varphi - \omega u^t) = \text{const}$. For simplicity, we take the angular momentum of the fluids to be zero (although our analysis can be readily extended to fluids with nonzero angular momentum). Then, $u_\pm^\varphi = \omega u_\pm^t$, and from the normalization condition $u_\mu u^\mu = -1$ we readily have $(\alpha u_\pm^t) = 1 + g_{rr}(u_\pm^r)^2 = 1 + u_\pm^2$, which simply defines the Lorentz factor of the fluid measured by a ZAMO, $\gamma_\pm = \alpha u_\pm^t$. Upon substituting the relation $\gamma_\pm^2 - 1 = u_\pm^2$ into Eq. (B7), using the orthogonality condition $s_\mu u^\mu = s_{\pm t} u_\pm^t + s_{\pm r} u_\pm^r = 0$, noting that $s_\pm^t = g^{tt} s_{\pm t} + g^{t\varphi} s_{\pm\varphi} = -s_{\pm t} / \alpha^2$, since we invoke $s_{\pm\varphi} = 0$, and transforming to the tortoise coordinate, we arrive at Eq. (10).

Appendix C: Radiation

1. Transport equation

In terms of the absorption coefficient κ_ν and the emissivity $g_\nu = c^2 j_\nu / (h^4 \nu^3)$, the transport equation for the photon distribution function, $f(x^\mu, p^\nu)$, takes the covariant form:

$$p^\alpha \partial_\alpha f - \Gamma_{\beta\gamma}^\alpha p^\beta p^\gamma \frac{\partial f}{\partial p^\alpha} = p^t (-\kappa_\nu f + g_\nu), \quad (\text{C1})$$

where $\Gamma_{\beta\gamma}^\alpha$ is the usual Christoffel symbol. With respect to a ZAMO frame defined by the tetrads $e_{\hat{t}} = \frac{1}{\alpha}(\partial_t + \omega\partial_\varphi)$, $e_{\hat{r}} = \frac{1}{\sqrt{g_{rr}}}\partial_r$, $e_{\hat{\theta}} = \frac{1}{\sqrt{g_{\theta\theta}}}\partial_\theta$, $e_{\hat{\varphi}} = \frac{1}{\sqrt{g_{\varphi\varphi}}}\partial_\varphi$, the components of the photon momentum are $p_{\hat{a}} = e_{\hat{a}}^b p_b$, and $p^{\hat{a}} = \eta^{\hat{a}\hat{b}} p_{\hat{b}}$. In this frame we define the direction vectors $n^{\hat{a}} = (1, \mu_p, \sin\theta_p \cos\varphi_p, \sin\theta_p \sin\varphi_p)$, where $\mu_p = \cos\theta_p$ [24]. Clearly $n_{\hat{a}} n^{\hat{a}} = 0$, as required. The photon momentum in this frame is $p^{\hat{a}} = \nu n^{\hat{a}}$, where henceforth we use units where $h = c = 1$. Note that the angle θ_p is measured with respect to the radial direction ∂_r . We suppose that the photon distribution is axi-symmetric locally, that is f is independent of φ_p . Then, the transfer equation takes the form [24, 25]

$$\left[n^{\hat{a}} \partial_{\hat{a}} - \gamma_{\hat{a}\hat{b}}^{\hat{t}} n^{\hat{a}} n^{\hat{b}} \nu \frac{\partial}{\partial \nu} + (n^{\hat{r}} \gamma_{\hat{a}\hat{b}}^{\hat{t}} - \gamma_{\hat{a}\hat{b}}^{\hat{r}}) n^{\hat{a}} n^{\hat{b}} \frac{\partial}{\partial \mu_p} \right] f = -\kappa_\nu f + g_\nu, \quad (\text{C2})$$

in terms of the Ricci rotation coefficients $\gamma_{\hat{b}\hat{c}}^{\hat{a}} = e_{\hat{b}}^\lambda e_{\hat{c}}^\nu (\partial_\nu e_{\hat{b}}^\lambda + \Gamma_{\nu\mu}^\lambda e_{\hat{b}}^\mu)$.

In applying the transport equation to the gamma ray emission in the gap we take $\nu = \epsilon_\gamma$, $\mu_p = \mu_\gamma$, $\varphi_p = \varphi_\gamma$, $f = I_\gamma(r, \epsilon_\gamma, \mu_\gamma)/\epsilon_\gamma^3$. Since the beamed intensity is independent of φ_γ we can average the transport equation over this angle. Using the relations

$$\gamma_{\hat{a}\hat{b}}^{\hat{t}} n^{\hat{a}} n^{\hat{b}} = n^{\hat{a}} \partial_{\hat{a}} \ln \alpha = \frac{\mu_\gamma}{\sqrt{g_{rr}}} \partial_r \ln \alpha \quad (\text{C3})$$

and

$$\frac{1}{2\pi} \int \gamma_{\hat{a}\hat{b}}^{\hat{t}} n^{\hat{a}} n^{\hat{b}} d\varphi_\gamma = \gamma_{\hat{t}\hat{t}}^{\hat{t}} + \frac{1}{2}(1 - \mu_\gamma^2)(\gamma_{\hat{\theta}\hat{\theta}}^{\hat{t}} + \gamma_{\hat{\varphi}\hat{\varphi}}^{\hat{t}}) = \frac{1}{\sqrt{g_{rr}}} [\partial_r \ln \alpha - (1 - \mu_\gamma^2) \partial_r \ln \sqrt{A}], \quad (\text{C4})$$

one finally arrives at:

$$n^{\hat{a}} \partial_{\hat{a}} I_\gamma - \frac{\mu_\gamma}{\sqrt{g_{rr}}} (\partial_r \ln \alpha) \epsilon_\gamma^4 \frac{\partial}{\partial \epsilon_\gamma} (I_\gamma / \epsilon_\gamma^3) + \left[-\partial_r \ln \alpha + \frac{1}{2} \partial_r \ln \sqrt{A} \right] \frac{(1 - \mu_\gamma^2)}{\sqrt{g_{rr}}} \frac{\partial}{\partial \mu_\gamma} I_\gamma = -\kappa_{pp} I_\gamma + j_\gamma. \quad (\text{C5})$$

To simplify our analysis we shall neglect the term $\partial_r \ln \alpha / \sqrt{g_{rr}}$ as it is merely important very near the horizon. we further apply the beaming approximation (14), note that $n^{\hat{a}} \partial_{\hat{a}} = \frac{1}{\sqrt{g_{rr}}} \partial_r$, and integrate the later equation over the angle μ_γ to obtain:

$$\frac{1}{\sqrt{A}} \partial_r (\sqrt{A} I_\gamma^\pm) = \sqrt{g_{rr}} (\pm \kappa_{pp} I_\gamma^\pm \mp j_\gamma^\pm). \quad (\text{C6})$$

Upon transforming to the tortoise coordinate we obtain Eq. (15).

2. Inverse Compton emissivity

We consider inverse Compton scattering of target radiation by a cold electron (positron) beam of comoving density n_\pm . The intensity of the target radiation, as measured in the rest frame of the beam, is denoted by $I'_s(\epsilon'_s, \mu'_s, r, t)$, with ϵ'_s, μ'_s being the energy and direction of the target photons. The comoving gamma-ray emissivity has the general form

$$j'_\gamma(\epsilon'_\gamma, \mu'_\gamma, r, t) = n_\pm \int \frac{\epsilon'_\gamma}{\epsilon'_s} I'_s(\epsilon'_s, \mu'_s, r, t) \frac{d\sigma'}{d\Omega'_\gamma} \delta[\epsilon'_\gamma - \epsilon'_c(\epsilon'_s)] d\epsilon'_s d\Omega'_s, \quad (\text{C7})$$

here

$$\epsilon'_c(\mu'_s) = \frac{\epsilon'_s}{1 + \frac{h\epsilon'_s}{m_e c^2} (1 - \cos \psi)}, \quad (\text{C8})$$

ψ is the angle between the incident and scattered photons, given by $\cos \psi = \mu'_\gamma \mu'_s + \sin \theta'_\gamma \sin \theta'_s \cos(\varphi'_\gamma - \varphi'_s)$, and

$$\frac{d\sigma'}{d\Omega'_\gamma} = \frac{3\sigma_T}{16\pi} \left(\frac{\epsilon'_\gamma}{\epsilon'_s} \right)^2 \left(\frac{\epsilon'_\gamma}{\epsilon'_s} + \frac{\epsilon'_s}{\epsilon'_\gamma} - \sin^2 \psi \right) \quad (\text{C9})$$

is the differential Klein-Nishina cross-section. In our model the target radiation field is taken to be isotropic in the ZAMO frame with a power law spectrum, $I_s = I_0(r)(\epsilon_s/\nu_{min})^{-p}$, $\epsilon_{min} < \epsilon_s < \epsilon_{max}$. Since the Lorentz factor of the

beams, γ_{\pm} , is extremely large, we safely assume that the target radiation field is completely beamed in the comoving frame. Specifically,

$$I_s^{\pm}(\epsilon'_s, \mu'_s, r) = \frac{4\gamma_{\pm}}{3} I_0(r) (\epsilon'_s/2\gamma_{\pm}\epsilon_{min})^{-p} \delta(1 \mp \epsilon'_s); \quad 2\gamma_{\pm}\epsilon_{min} < \epsilon'_s < 2\gamma_{\pm}\epsilon_{max}, \quad (C10)$$

where superscript $+$ ($-$) refers to the positron (electron) beam. Performing the integral in Eq. (C7) and noting that $|d\epsilon'_c/d\epsilon'_s| = (\epsilon'_c/\epsilon'_s)^2$ yields:

$$j_{\gamma}^{\pm}(\epsilon'_\gamma, \mu'_\gamma, r) = \frac{\sigma_T n_{\pm}}{2} I_0(\epsilon'_s/2\gamma_{\pm}\epsilon_{min})^{-p} \frac{\epsilon'_\gamma}{\epsilon'_s} \left[\frac{\epsilon'_\gamma}{\epsilon'_s} + \frac{\epsilon'_s}{\epsilon'_\gamma} - 1 + \mu'^2_\gamma \right]. \quad (C11)$$

Transforming back to the ZAMO frame, and recalling that

$$\epsilon'_\gamma/\epsilon'_s = 1 - \epsilon_\gamma(1 - \beta_{\pm})\gamma_{\pm}(1 + \mu_\gamma), \quad \frac{\epsilon'_s}{2\gamma_{\pm}\epsilon_{min}} = \frac{\epsilon_\gamma}{2\epsilon_{min}} \left[\frac{1 - \beta_{\pm}\mu_\gamma}{1 - \epsilon_\gamma\gamma_{\pm}(1 - \beta_{\pm})(1 + \mu_\gamma)} \right],$$

we have

$$j_{\gamma}^{\pm}(\epsilon_\gamma, \mu_\gamma, r) = \frac{j_{\gamma}^{\pm}(\epsilon'_\gamma, \mu'_\gamma, r)}{[\gamma_{\pm}(1 - \beta_{\pm}\mu_\gamma)]^2} = \frac{\sigma_T n_{\pm}\gamma_{\pm}}{2} I_0(r) (\epsilon_\gamma/2\epsilon_{min})^{-p} g(\epsilon_\gamma, \mu_\gamma, \gamma_{\pm}), \quad (C12)$$

where

$$g(\epsilon_\gamma, \mu_\gamma, \gamma_{\pm}) = \frac{1}{\gamma_{\pm}^2(1 - \beta_{\pm}\mu_\gamma)^2} \left[\frac{2\gamma_{\pm} - \epsilon_\gamma(1 + \mu_\gamma)}{2\gamma_{\pm}(1 - \beta_{\pm}\mu_\gamma)} \right]^p \frac{\epsilon'_\gamma}{\epsilon'_s} \left[\frac{\epsilon'_\gamma}{\epsilon'_s} + \frac{\epsilon'_s}{\epsilon'_\gamma} - 1 + \mu'^2_\gamma \right].$$

Noting that the minimum and maximum scattering angles for a given gamma ray energy are

$$1 - \beta_{\pm}\mu_{min} = \min \left[(1 + \beta_{\pm}), \frac{2\epsilon_{max}}{\epsilon_\gamma} - \frac{2\epsilon_{max}}{\gamma_{\pm}} \right], \quad (C13)$$

$$1 - \beta_{\pm}\mu_{max} = \max \left[(1 - \beta_{\pm}), \frac{2\epsilon_{min}}{\epsilon_\gamma} - \frac{2\epsilon_{min}}{\gamma_{\pm}} \right],$$

and averaging the emissivities over angles, that is,

$$j_{\gamma}^{\pm}(\epsilon_\gamma, r) = \frac{1}{2} \int_{\mu_{min}}^{\mu_{max}} j_{\gamma}^{\pm}(\epsilon_\gamma, \mu_\gamma, r) d\mu_\gamma, \quad (C14)$$

one obtains, to leading order, the beamed emissivities in Eq. (19).

Appendix D: Derivation of $\langle Q_{cur} \rangle$

As argued below Eq. (38), at energies $\epsilon_\gamma < \epsilon_c$ the pair production opacity is much smaller than unity. We can therefore neglect absorption in the transfer equation (15). We can also neglect the IC emissivity since it is much smaller than the curvature emissivity at these energies. The approximate solutions to Eq. (38), subject to the boundary conditions (32), then read:

$$I_{\gamma}^{+}(r, \epsilon_\gamma) = -\frac{\sqrt{3}\alpha_f}{2\pi R_c} \gamma_{+} F(\epsilon_\gamma/\epsilon_c) \frac{1}{\sqrt{A(r)}} \int_r^{r_{out}} \frac{\sqrt{A} N_{+}^r}{\Delta} dr', \quad (D1)$$

$$I_{\gamma}^{-}(r, \epsilon_\gamma) = \frac{\sqrt{3}\alpha_f}{2\pi R_c} \gamma_{-} F(\epsilon_\gamma/\epsilon_c) \frac{1}{\sqrt{A(r)}} \int_{r_{in}}^r \frac{\sqrt{A} N_{-}^r}{\Delta} dr'. \quad (D2)$$

We note that $\sqrt{A(r)}$ changes by at most a factor of 3 across the gap, so we assume it is constant with an average value $\langle \sqrt{A} \rangle = (\sqrt{A_{in}} + \sqrt{A_{out}})/2$, where $A_{in} \equiv A(r_{in})$ and likewise for A_{out} . Recalling that $N_{+}^r - N_{-}^r = N_0^r = \text{const}$, and that $\gamma^{+} = \gamma^{-} \equiv \gamma$ across most of the gap, and taking $\langle \sqrt{A} \rangle$ instead of $\sqrt{A(r)}$, the sum of the two intensities yields

$$I_{\gamma}^{+}(r_{in}, \epsilon_\gamma) + I_{\gamma}^{-}(r_{out}, \epsilon_\gamma) = \frac{\sqrt{3}\alpha_f}{2\pi R_c} \gamma F(\epsilon_\gamma/\epsilon_c) (-N_0^r) \frac{1}{\langle \sqrt{A} \rangle} \int_{r_{in}}^{r_{out}} \frac{\sqrt{A} dr'}{\Delta} \quad (D3)$$

With the crude approximation $I_\gamma^+(r, \epsilon_\gamma) + I_\gamma^-(r, \epsilon_\gamma) = [I_\gamma^+(r_{in}, \epsilon_\gamma) + I_\gamma^-(r_{out}, \epsilon_\gamma)]/2$, we obtain an expression for the average pair production rate:

$$\langle Q_{cur} \rangle = \frac{\sqrt{27}\alpha_f}{2R_c} \gamma \tau_0 (-N_0^r) A_p (\epsilon_c \epsilon_{min})^p \frac{1}{\langle \sqrt{A} \rangle} \int_{r_{in}}^{r_{out}} \frac{\sqrt{A} dr'}{2\Delta} \int_0^\infty x^{p-1} F(x) dx. \quad (D4)$$

By employing Eqs. (33) and (35), choosing $p = 2$ for illustration, and computing the last integral on the right hand side we arrive at Eq. (39).

-
- | | |
|---|--|
| <p>[1] R. D. Blandford and R. L. Znajek, Mon. Not. R. Astron. Soc., 179, 433, (1977)</p> <p>[2] M. Barkov and S. Komissarov, Mon. Not. R. Astron. Soc., 385, L28 (2008)</p> <p>[3] A. Levinson and F. Rieger, Astrophys. J., 730, 123 (2011)</p> <p>[4] A. Levinson, PhRvL, 85, 912 (2000)</p> <p>[5] K. Hirotani, Pu H.-Y., 2016, Astrophys. J., 818, 50 (2016)</p> <p>[6] K. Hirotani, H.-Y. Pu, L. C.-C. Lin, H.-K. Chang, M. Inoue, A. K. H. Kong, S. Matsushita and P.-H. T. Tam, Astrophys. J., 833, 142 (2016)</p> <p>[7] K. Hirotani, H.-Y. Pu, L. C.-C. Lin, A. K. H. Kong, S. Matsushita, K. Asada, H.-K. Chang and P.-H. T. Tam, Astrophys. J., 845, 77 (2017)</p> <p>[8] L. C.-C. Lin, H.-Y. Pu, K. Hirotani, A. K. H. Kong, S. Matsushita, H.-K. Chang, M. Inoue and P.-H. T. Tam, Astrophys. J., 845, 40 (2017)</p> <p>[9] A. Neronov, F. A. Aharonian, Astrophys. J., 671, 85 (2007)</p> <p>[10] F. M. Rieger, Int. J. Mod. Phys. D, 20, 1547 (2011)</p> <p>[11] A. E. Broderick and A. Tchekhovskoy, Astrophys. J., 809, 97 (2015)</p> <p>[12] F. A. Aharonian, et al., Astron. Astrophys., 403, L1 (2003)</p> <p>[13] V. A. Acciari, et al., Sci, 325, 444 (2009)</p> | <p>[14] J. Aleksić, et al., Sci, 346, 1080 (2014)</p> <p>[15] A. Y. Chen and A. M. Beloborodov, Astrophys. J., 795, L22 (2014)</p> <p>[16] B. Cerutti, A. Philippov, K. Parfrey and A. Spitkovsky, Mon. Not. R. Astron. Soc., 448, 606 (2015)</p> <p>[17] A. A. Philippov, A. Spitkovsky and B. Cerutti, Astrophys. J., 801, L19 (2015)</p> <p>[18] N. Globus and A. Levinson, Astrophys. J., 796, 26 (2014)</p> <p>[19] N. Globus and A. Levinson, PhRvD, 88, 084046 (2013)</p> <p>[20] R. Narayan and I. Yi, Astrophys. J., 452, 710 (1995)</p> <p>[21] R. D. Blandford and A. Levinson, Astrophys. J., 441, 79 (1995)</p> <p>[22] G. B. Rybicki and A. P. Lightman, Radiative Processes in Astrophysics (New York: Wiley) (1979)</p> <p>[23] R. J. Gould and G. P. Schröder, PhRv, 155, 1404 (1967)</p> <p>[24] K. Morita and N. Kaneko, Astrophys. & Space Sci., 121, 105 (1986)</p> <p>[25] R. W. Lindquist, AnPhy, 37, 487 (1966)</p> <p>[26] M. Takahashi, S. Nitta, Y. Tatematsu & A. Tomimatsu, Astrophys. J., 363, 206 (1990)</p> <p>[27] A. Levinson, D. Melrose, A. Judge & L. Qinghuan, Astrophys. J., 631, 456 (2005)</p> <p>[28] A. N. Timokhin & J. Arons, Mon. Not. R. Astron. Soc., 429, 20 (2013)</p> |
|---|--|